JOURNAL OF AIRCRAFT
Vol. 43, No. 4, July–August 2006

Aeroservoelastic Modeling and Sensitivity Analysis with Strain Actuators

Moti Karpel* and Boris Moulin†
Technion–Israel Institute of Technology, 32000 Haifa, Israel

DOI: 10.2514/1.19279

Mathematical models of aeroservoelastic systems are expanded to facilitate the use of distributed strain actuators in automated design processes. Strain actuators, such as piezoelectric patches, can change the shape of lifting surfaces by introducing structural strains due to electric voltage commands. The voltage–strain relations, the overdetermined nature of the elastic actuator-structure equilibrium, the relatively large number of involved interface coordinates, and the high importance of local strains that typically limit the actuator performance require substantial modifications in the modeling process compared with that with common control-surface actuators. A control mode is defined by the static deformations due to a unit static voltage command. Huge dummy masses are used to generate the control modes and their mass coupling with the elastic modes as part of a standard normal-modes analysis. State-space aeroservoelastic equations are constructed using the minimum-state rational aerodynamic approximation approach. Analytical expressions are given for the sensitivity of the system coefficient matrices and the associated aeroservoelastic stability and response parameters with respect to the actuator properties. A numerical application of an unmanned aerial vehicle with a piezoelectric-driven control surface is given. The example demonstrates the modeling process, some aeroelastic response parameters to control commands, and the associated sensitivity analysis.

I. Introduction

THE use of strain actuators to control the structural dynamic stability and response of air vehicles is a branch of the emerging smart-structure technology that attracted extensive research and development efforts in recent years [1–3]. Strain actuators, such as those based on piezoelectric patches, are embedded in the structure and subjected to electric inputs that cause the structure to change its shape. The shape changes introduce internal forces that deform the surrounding structure and affect its aeroelastic behavior. A control system that assigns electric commands according to sensor readings via a control law closes the aeroservoelastic (ASE) loop.

Common ASE modeling techniques, such as that of [4] that formed the basis for the ASE module in the ZAERO software package [5], assume that the surface shape is controlled by use of standard control surfaces that are connected in rotation to the structure by a statically determined manner. A control mode in this case, which is defined as the air-off shape change due to a static unit control command, is a kinematic mode defined by the structure geometry and the rotation axis. Control modes associated with strain actuators are more difficult to define due to the voltage–strain relations, the overdetermined nature of the elastic actuator-structure equilibrium and the relatively large number of involved interface coordinates. Another major problem is that the standard modal approach might not consider the deformations at and near the smart components adequately. These deformations might be vital for a proper evaluation of the performance of the strain actuators and their structural integrity.

The ASE modeling technique of [4] was expanded in [6] facilitate strain actuators. Two approaches were presented: one that uses control modes and one that bypasses the need for control modes by using direct excitation forces extracted from the strain–voltage relations and the structural dynamic response. Both approaches were based on the use of fictitious masses when the structural modes are generated. The fictitious-mass (FM) method [7,8] is used to enforce selected local deformations in the set of low-frequency modes taken into account in the modal-based analysis. The normal modes are calculated with selected degrees of freedom loaded by large fictitious masses. Their dynamic effects are later removed, leaving the modal basis with a set of local deformation modes to be included in the subsequent modal-based analyses.

The effectivity of the FM method is reduced with increasing number of fictitious masses in the model, because it requires a greater number of modes to be taken into account, which increases the size of the resulting model. Reference [6] showed that this might be a problem in smart-structure applications when the direct-force approach is used because the adequate number of interface coordinates between the piezoelectric patches and the structure can be relatively large. It also showed that the balance of internal forces in the patches facilitates the application of special FM matrices that reduce the number of added modes. It was suggested to attach to each patch a fictitious-mass matrices which is proportional to the stiffness matrix of the patch. The resulting models exhibited high-accuracy local stresses in subsequent analyses with a minimal number of added modes. However, it was also showed that the expanded modal data base might cause numerical difficulties in the aerodynamic rational approximation process that is needed for aeroservoelastic analysis. The control-mode approach in [6] was based on using only one huge fictitious mass for each piezoelectric patch, mounted on a scalar point that represents the voltage input.

The purpose of this paper is to generalize and expand the control-mode approach; to present a convenient way for generating them; to develop the necessary formulation for subsequent aeroservoelastic analysis, sensitivity studies, and design optimization; and to demonstrate the application of the new developments.

II. Strain Actuator Forces

Strain actuators are structural components that cause strains and deformations in the surrounding structure as a result of changing their shape when subjected to some input commands. This

Presented as Paper 2078 at the AIAA/ASME/ASCE/AHS/ASC 46th Structures, Structural Dynamics and Materials Conference, Austin, TX, 18–21 April 2005; received 1 August 2005; revision received 3 November 2005; accepted for publication 26 November 2005.

*Professor, Sanford Kaplan Chair for Aerospace Engineering, Faculty of Aerospace Engineering. Associate Fellow AIAA.

†Senior Researcher, Faculty of Aerospace Engineering. Member AIAA.

work relates to elastic piezoelectric patches that change their shape when subjected to electric voltage commands. The modeling methodology, however, is applicable to all kinds of actuators, from the statically determined ones to complex piezoelectric patches embedded in the structure. A patch is characterized by the displacement vector of its interface grid points $\{x_{p_i}\}$ due to a unit voltage input, when the patch is not attached to the structure but still may be restrained in a statically determined manner. It is assumed at this stage that the dependency of $\{x_{p_i}\}$ on the associated voltage input v_i is linear and independent of the excitation frequency. Other displacement-voltage dependencies can be modeled later as part of the control system or by introducing nonlinear structured elements, which are beyond the scope of this paper.

When attached to the structure, the patch deformations are, of course, functions of the external loads and the elastic properties of the structure. The discrete elastic forces applied in this case by a piezoelectric patch to the structure are

$$\{F_{p_i}(t)\} = [\bar{K}_{pp_i}](\{x_{p_i}\}v_i(t) - \{u_{p_i}(t)\}) \tag{1}$$

where $[\bar{K}_{pp_i}]$ is the free-free stiffness matrix of the ith patch and $\{u_{p_i}\}$ is the actual displacement vector at the patch–structure interface grid points.

With the stiffness matrices of the piezoelectric patches added to the stiffness matrix of the structure, the static equilibrium equation of the structure under loads generated by static voltage commands is

$$[K_{aa}]\{u_a\} = \{F_a\} \tag{2}$$

where

$$[K_{aa}] = \begin{bmatrix} K_{ll} & K_{lp} \\ K_{lp}^T & K_{pp} + K_{pp}^p \end{bmatrix}$$

$$\{u_a\} = \begin{Bmatrix} u_l \\ u_p \end{Bmatrix}, \qquad \{F_a\} = \begin{bmatrix} 0 \\ K_{pp}^p \end{bmatrix}[X_{pv}]\{v\}$$

where subscript a relates to all the free degrees of freedom of the structure, subscript p relates to the degrees of freedom at which the actuators are connected, and subscript l to the other degrees of freedom of the displacement vector $\{u_a\}$, $[K_{pp}^p]$ is the assembly of the stiffness matrices $[\bar{K}_{pp_i}]$ of the patches, $[X_{pv}]$ is the assembly of all the patch unit-command displacements $\{x_{p_i}\}$, and $\{v\}$ is the vector of piezoelectric voltage inputs. The forces in the right-hand side of Eq. (2) are those obtained when the patched are connected to a rigid structure. Piezoelectric devices are often characterized by the maximal values of these forces.

The assembly of the displacement vectors $[\phi_{av}]$ that satisfy Eq. (2) with separate unit voltage commands, namely

$$[K_{aa}][\phi_{av}] = \begin{bmatrix} 0 \\ K_{pp}^p \end{bmatrix}[X_{pv}] \tag{3}$$

is called here the matrix of *piezoelectric control modes*. It can be solved within a static finite-element solution with the right side defined as a set of loading vector. The singularity of $[K_{aa}]$ in the case of a free-free structure can be resolved by the application of statically determined constraints. Since the right-hand force vectors are self-balanced, namely sum to zero total forces and moments in all directions, the constraints do not impose local constraint forces. The resulting static solution should then be modified by adding rigid-body displacements such that the deformations will preserve the location and orientation of the center of mass, which implies orthogonality with the free-free rigid-body modes $[\phi_{ar}]$

$$[\phi_{ar}]^T[M_{aa}][\phi_{av}] = \{0\} \tag{4}$$

A convenient way for obtaining the control modes as part of a standard normal-modes analysis is discussed below. This option simplifies the subsequent aeroservoelastic formulation, as discussed in the following sections.

III. Generation of Control Modes

The method of obtaining piezoelectric control modes and the associated generalized matrices in standard finite-element codes such as MSC/NASTRAN is an extension and generalization of the method for obtaining common control-surface modes described in [4]. Common control surfaces are connected to the aircraft structure through statically determined rotation connections. The control-mode generation method in this case is based on the introduction of huge fictitious masses. The finite-element model is modified such that, first, each control surface is disconnected from its actuator. The differential motion between the two sides of each disconnection point defines a new degree of freedom δ_i that represents the rigid-body rotation of the control surface relative to the wing. The δ_i coordinates (one per control surface) are loaded with fictitious masses of very large magnitudes, typically orders of magnitude larger than the entire aircraft. A standard normal-modes analysis is then performed for obtaining the natural frequencies and the associated normal modes in the frequency range of interest required for flutter analysis. The resulting normal modes include the control modes as structural modes with almost-zero natural frequencies, whereas the other modes and their associated natural frequencies and generalized masses are practically equal to those of the original structure, including rigid-body modes.

The technique for generating control modes is expanded here to be applicable to strain actuators with overdetermined connections to the structure. The expanded procedure starts in the finite-element modeling. The actuator-structure interface grid points are duplicated with one set remaining connected to the structure, and the other set connected to the actuators (piezoelectric elements in our case) only. A scalar point whose displacement v_i represents the voltage input is added to the model for each piezoelectric patch. At this point the structure is disconnected from the actuators such that the static equilibrium with no external forces is

$$\begin{bmatrix} K_{ll} & K_{lp} & 0 & 0 \\ K_{lp}^T & K_{pp} & 0 & 0 \\ 0 & 0 & K_{pp}^p & 0 \\ 0 & 0 & 0 & 0 \end{bmatrix} \begin{Bmatrix} u_l \\ u_p \\ \bar{u}_p \\ v \end{Bmatrix} = \{0\} \tag{5}$$

where $\{\bar{u}_p\}$ is the vector of actuator-side displacements of the actuator-structure connections. To connect the actuator, the actuator-side displacements are connected to the structure-side ones by the multipoint constraint (MPC) equations

$$\{\bar{u}_p\} = \{u_p\} - [X_{pv}]\{v\} \tag{6}$$

which is, of course, in contradiction with the fact that the structure-side and the actuator-side displacements are equal. However, in this way the actuator displacements $\{\bar{u}_p\}$ yield actuator stresses and strains that include the piezoelectric effects.

The elimination of $\{\bar{u}_p\}$ from Eq. (5), using the MPC constraints of Eq. (6), and the addition of a generalized piezoelectric force vector $\{F_v\}$ (one force per piezoelectric patch) that drives $\{v\}$ yield

$$\begin{bmatrix} K_{ll} & K_{lp} & 0 \\ K_{lp}^T & K_{pp} + K_{pp}^p & -K_{pp}^p X_{pv} \\ 0 & -X_{pv}^T K_{pp}^p & X_{pv}^T K_{pp}^p X_{pv} \end{bmatrix} \begin{Bmatrix} u_l \\ u_p \\ v \end{Bmatrix} = \begin{Bmatrix} 0 \\ 0 \\ F_v \end{Bmatrix} \tag{7}$$

It can be observed that the top two partitions of Eq. (7) combine for Eq. (2). The control mode can now be calculated by n_v static solutions of Eq. (7) with one term in $\{F_v\}$ is $F_{v_i} = 1$ and the others are 0, modified by the addition of rigid-body modes such that Eq. (4) is satisfied, and followed by the normalization of the resulting displacement vectors such that $v_i = 1$. It is more convenient, however, to extract these modes by loading the scalar points by very large masses $[M_H]$ and calculating the normal modes using standard routines, as suggested in [6]. The resulting normal modes include n_v control modes of practically zero frequency, whereas the other modes are practically identical to those of the original structure.

It is shown below that the resulting control modes satisfy the orthogonality requirement of Eq. (4). To normalize and separate the control modes such that they become consistent with Eq. (3), their modal displacements can be partitioned into structural displacements $[\bar{\phi}_{av}]$ and scalar-point displacements $[\bar{\phi}_{Hv}]$, which is an $n_v \times n_v$ matrix. The n_v desired control modes $[\phi_{av}]$ of Eq. (3) are calculated by

$$[\phi_{av}] = [\bar{\phi}_{av}][\bar{\phi}_{Hv}]^{-1} \tag{8}$$

In this way the scalar-point partition of the control modes becomes $[\phi_{Hv}] = [I]$. Orthogonality implies that the other normal modes $[\phi_{ah}]$ are related to the control modes by

$$\begin{bmatrix} \phi_{ah} \\ \phi_{Hh} \end{bmatrix}^T \begin{bmatrix} M_{aa} & 0 \\ 0 & M_H \end{bmatrix} \begin{bmatrix} \phi_{av} \\ I \end{bmatrix} = [0] \tag{9}$$

where $[\phi_{Hh}]$ contains the participation of the scalar points in the structural modes. Because of the huge masses in $[M_H]$, the displacements in $[\phi_{Hh}]$ are negligible compared with the other structural displacements in these modes. However, when multiplied by $[M_H]$ they are significant and useful for a convenient calculation of the mass coupling matrix $[M_{hv}]$ between the structural and the control modes, as can be extracted from Eq. (9),

$$[M_{hv}] = [\phi_{ah}]^T[M_{aa}][\phi_{av}] = -[\phi_{Hh}]^T[M_H] \tag{10}$$

where the right-hand expression can be easily extracted directly from the modal data. The rigid-body modes $[\phi_{ar}]$ are a subset of $[\phi_{ah}]$. Since $[\phi_{ar}]$ contain no elastic strains, the associated scalar-point modal displacements are $[\phi_{Hr}] = [0]$, which proves that the control modes satisfy the constraint conditions of Eq. (4).

IV. Aeroservoelastic Equations of Motion

Once piezoelectric control modes are defined, the aeroservoelastic equations of motion can be constructed in the same manner as they are constructed with conventional actuator-driven control surfaces. The aeroservoelastic equations of motion can be expressed in either the time domain [4] or the frequency domain [9]. The main advantage of the frequency-domain approach is that the aerodynamic force coefficient (AFC) matrices can keep their traditional transcendental frequency-dependent form. In contrast, the time-domain equations require the AFC matrices to be approximated as rational functions in the Laplace domain. Whereas there might be some loss of accuracy associated with the rational approximations, the time-domain equations are more suitable for application of modern control and simulation methods and gradient-based optimization techniques [10].

The rational approximation of the unsteady AFC matrices, in the Laplace domain, is of the form

$$[\tilde{Q}_h(s)] = [A_{h0}] + \frac{b}{V}[A_{h1}]s + \frac{b^2}{V^2}[A_{h2}]s^2 + [D_h]\left([I]s - \frac{V}{b}[R]\right)^{-1}[E]s \tag{11}$$

where the $[A_{hi}]$ and $[E]$ matrices are column partitioned according to the structural and control modes as

$$[A_{hn}] = [A_{hh_n} A_{hv_n}] \qquad (n = 0, 1, 2); \qquad [E] = [E_h E_v]$$

Several approximation techniques are available for obtaining the coefficient matrices in Eq. (11). The techniques apply least square solutions that approximate a set of force coefficients matrices $[Q_h(ik)]$ determined for harmonic oscillations at several tabulated reduced-frequency values $k = \omega b/V$, where ω is the frequency of oscillations, b is a reference semichord, and V is the air velocity.

The resulting state-space equation of motion of the open-loop aeroelastic system excited by piezoelectric voltage inputs $\{v(t)\}$ is

$$\{\dot{x}_{ae}\} = [A_{ae}]\{x_{ae}\} + [B_{ae}]\{u_{ae}\} \tag{12}$$

where

$$\{x_{ae}\} = \begin{Bmatrix} \xi \\ \dot{\xi} \\ x_{\text{lag}} \end{Bmatrix}; \qquad \{u_{ae}\} = \begin{Bmatrix} v \\ \dot{v} \\ \ddot{v} \end{Bmatrix}$$

where $\{\xi\}$ is the vector of n_h modal displacements taken into account and $\{x_{\text{lag}}\}$ is the vector of n_{lag} aerodynamic lag states where n_{lag} is the size of $[R]$ in Eq. (10), and

$$[A_{ae}] = \begin{bmatrix} 0 & [I] & 0 \\ -[\bar{M}]^{-1}[\bar{K}] & -[\bar{M}]^{-1}[\bar{B}] & -q[\bar{M}]^{-1}[D_h] \\ 0 & [E_h] & \frac{V}{b}[R] \end{bmatrix}$$

$$[B_{ae}] = \begin{bmatrix} 0 & 0 & 0 \\ -[\bar{M}]^{-1}[\bar{K}_{hv}] & -[\bar{M}]^{-1}[\bar{B}_{hv}] & -[\bar{M}]^{-1}[\bar{M}_{hv}] \\ 0 & [E_v] & 0 \end{bmatrix}$$

where

$$[\bar{M}] = [M_{hh}] + \frac{qb^2}{V^2}[A_{hh_2}], \qquad [\bar{K}] = [K_{hh} + qA_{hh_0}]$$

$$[\bar{B}] = \left[B_{hh} + \frac{qb}{V}A_{hh_1}\right], \qquad [\bar{M}_{hv}] = \left[M_{hv} + \frac{qb^2}{V^2}A_{hv_2}\right]$$

$$[\bar{K}_{hv}] = q[A_{hv_0}], \qquad [\bar{B}_{hv}] = \frac{qb}{V}[A_{hv_1}]$$

The output parameters are expressed in the form

$$\{y_{ae}\} = [C_{ae}]\{x_{ae}\} + [D_{ae}]\{u_{ae}\} \tag{13}$$

Structural displacements, velocities, and accelerations can be cast in the form of Eq. (13) by the mode-displacement approach. Stresses and strains, which are often critical parameters in the performance evaluation of piezoelectric actuators, can also be adequately expressed in terms of modal displacements and the voltage inputs. The element strains, for example, are expressed by

$$\{\epsilon\} = [EU_a][\phi_{av}\phi_{ah}]\begin{Bmatrix} v \\ \xi \end{Bmatrix} = [\phi_{\epsilon v}\phi_{\epsilon h}]\begin{Bmatrix} v \\ \xi \end{Bmatrix} \tag{14}$$

where $[\phi_{\epsilon v}]$ and $[\phi_{\epsilon h}]$ are the modal strain matrices that can be extracted in the normal-modes analysis where the control mode and the structural modes are generated simultaneously.

As in the case of common control surfaces and actuators, the piezoelectric commands should also be modeled as driving the patch through a 3rd order filter (actuator) [5,11]. This is done to allow a proper representation of the mass coupling effects due to $[M_{hv}]$ without having a direct link between the command and the state response. The filters add three states for each piezoelectric patch. The roots of this filter should be far enough from those of the aeroelastic plant to avoid nonrealistic interference with the structural response, but not too far to avoid numerical difficulties in the subsequent simulations.

The main advantages of the control-mode approach compared with the direct-force approach presented in [6] are that a) local vibration modes generated by additional fictitious masses at the patch–structure connections are not essential as it is in the direct-force approach; b) the explicit appearance of the control columns in the aerodynamic approximation of Eq. (11) may improve their accuracy; and c) the modal data needed to construct the state-space equations can be extracted from a single standard normal-modes analysis of the structural model, which facilitates a convenient application in common ASE analysis codes such as ZAERO [5].

V. Optimization with a Fixed Modal Basis

Gradient-based aeroservoelastic design optimization procedures that are based on state-space time-domain formulation were presented and discussed in [10,11]. For the sake of efficiency, major design cycles are performed in these procedures with a fixed set of modal coordinates without returning to the full finite-element model.

The behavior functions and the optimization constraints, and their derivatives with respect to structural and control design variables, are updated along the design path based on modal sensitivity data prepared ahead of time by the finite-element code, while calculating the normal modes. The required formulation is based on the updated system matrices in Eqs. (12) and (13) and their derivatives with respect to the design variables. The sensitivity expressions of [10,11] are complemented in this section with system matrix derivatives with respect to the piezoelectric patch variables, which facilitates the associated sensitivities of all the ASE stability and response parameters discussed in [10,11].

While the normal modes of the baseline structure are used as a fixed set of modal coordinates, the piezoelectric control modes have to be changed in each design step because of their dependency on the elastic equilibrium between the structural deformation and the voltage command expressed in Eqs. (2) and (3). However, the fixed-modal-basis concept of [10] can still be used to express the control modes $[\tilde{\phi}_{av}]$ along the design path as a linear combination of baseline control and elastic modes

$$[\tilde{\phi}_{av}] = [\phi_{av}][\psi_{vv}] + [\phi_{ar}][\psi_{rv}] + [\phi_{ae}][\psi_{ev}] \tag{15}$$

where $[\phi_{ar}]$ and $[\phi_{ae}]$ are the rigid-body and the elastic partitions of $[\phi_{ah}]$. For the baseline structure, $[\psi_{vv}] = [I]$, $[\psi_{rv}] = [0]$ and $[\psi_{ev}] = [0]$. They are to be updated along the design path such that Eqs. (3) and (4) are satisfied for the updated structure. The substitution of Eq. (15) in Eq. (3) with updated stiffness terms, and the premultiplication by $[\phi_{av}\phi_{ae}]^T$ yields

$$\begin{bmatrix} \tilde{K}_{vv} & \tilde{K}_{ve} \\ \tilde{K}_{ve}^T & \tilde{K}_{ee} \end{bmatrix} \begin{bmatrix} \psi_{vv} \\ \psi_{ev} \end{bmatrix} = \begin{bmatrix} \phi_{pv}^T \\ \phi_{pe}^T \end{bmatrix} [\tilde{K}_{pp}^p][X_{pv}] \tag{16}$$

where the subscript p is as defined after Eq. (2) and

$$\begin{bmatrix} \tilde{K}_{vv} & \tilde{K}_{ve} \\ \tilde{K}_{ve}^T & \tilde{K}_{ee} \end{bmatrix} = \begin{bmatrix} K_{vv} & K_{ve} \\ K_{ve}^T & K_{ee} \end{bmatrix} + \begin{bmatrix} \Delta K_{vv} & \Delta K_{ve} \\ \Delta K_{ve}^T & \Delta K_{ee} \end{bmatrix}$$
$$[\tilde{K}_{pp}^p] = [K_{pp}^p] + [\Delta K_{pp}^p] \tag{17}$$

where $[K_{ee}]$ and $[K_{vv}]$ are the diagonal matrices of generalized stiffness values associated with the elastic and control modes, and $[K_{ve}]$ is the stiffness coupling between the elastic and control modes. As deduced from Eq. (3),

$$[\, K_{vv} \quad K_{ve} \,] = [X_{pv}]^T [K_{pp}^p] [\, \phi_{pv} \quad \phi_{pe} \,] \tag{18}$$

which can be easily calculated after the baseline normal-modes extraction using the stiffness matrices of the piezoelectric patches. The incremental (Δ) matrices in Eq. (17) are calculated during the optimization cycle. When the dependency of $[K_{aa}]$ on a design variable p_k is linear,

$$\begin{bmatrix} \Delta K_{vv} & \Delta K_{ve} \\ \Delta K_{ve}^T & \Delta K_{ee} \end{bmatrix} = \sum_k \frac{\partial}{\partial p_k} \begin{bmatrix} \tilde{K}_{vv} & \tilde{K}_{ve} \\ \tilde{K}_{ve}^T & \tilde{K}_{ee} \end{bmatrix} p_k \tag{19}$$

where

$$\frac{\partial}{\partial p_k} \begin{bmatrix} \tilde{K}_{vv} & \tilde{K}_{ve} \\ \tilde{K}_{ve}^T & \tilde{K}_{ee} \end{bmatrix} = \begin{bmatrix} \phi_{av}^T \\ \phi_{ae}^T \end{bmatrix} \frac{\partial [K_{aa}]}{\partial p_k} [\phi_{av} \phi_{ae}] \tag{20}$$

which can be calculated when the baseline modes are generated. The treatment of structural design variables that have quadratic effects of the stiffness matrix, such thickness effects on out-of-plane stiffness of plates, is discussed in [10]. The generalized mass, stiffness and damping matrices in $[A_{ae}]$ and $[B_{ae}]$ of Eq. (12) are updated in a similar way, using the associated derivatives with respect to the design variables stored in the modal data base [10].

The solution of Eq. (16) at each step along the optimization path provides the updated $[\psi_{vv}]$ and $[\psi_{ev}]$ of Eq. (15). The substitution of Eq. (15) in Eq. (4) yields the updated $[\psi_{rv}]$,

$$[\psi_{rv}] = -[\tilde{M}_{rr}]^{-1} (\Delta[M_{rv}][\psi_{vv}] + [\tilde{M}_{re}][\psi_{ev}]) \tag{21}$$

where $[\tilde{M}_{rr}]$ and $[\tilde{M}_{re}]$ are calculated similarly to $[\tilde{K}_{ee}]$ in Eq. (17) and $\Delta[M_{rv}]$ similarly to $\Delta[K_{ve}]$ in Eq. (19). With this update performed in each iteration, the rigid-body partition of the mass coupling matrix of Eq. (10) remains zero throughout the design path and the elastic-mode partition becomes

$$[\tilde{M}_{ev}] = ([M_{ev}] + \Delta[M_{ev}])[\psi_{vv}] + [\tilde{M}_{er}][\psi_{rv}] + [\tilde{M}_{ee}][\psi_{ev}] \tag{22}$$

where $\Delta[M_{ev}]$, $[\tilde{M}_{er}]$, and $[\tilde{M}_{ee}]$ are calculated similarly to $\Delta[M_{rv}]$, $[\tilde{M}_{rr}]$, and $[\tilde{M}_{re}]$.

The control-related matrices in $[B_{ae}]$ of Eq. (12) (those that have v as their second subscript) are updated along the optimization path according to the mass coupling of Eq. (22) and with the updated control-mode-related aerodynamic terms

$$[\tilde{A}_{hv_i}] = [A_{hv_i}][\psi_{vv}] + [A_{hh_i}][\psi_{hv}] \tag{23}$$

and

$$[\tilde{E}_v] = [E_v][\psi_{vv}] + [E_h][\psi_{hv}] \tag{24}$$

where only $[\psi_{vv}]$ and $[\psi_{hv}] = [\psi_{rv}\psi_{ev}]$ change along the design path.

The update of the output matrices in Eq. (13) should also consider the changes of the control modes $[\tilde{\phi}_{av}]$ according to Eq. (15). Strain outputs, for example, are updated by

$$[\tilde{\phi}_{\epsilon v}] = [\phi_{\epsilon v}][\psi_{vv}] + [\phi_{\epsilon h}][\psi_{hv}] \tag{25}$$

It should be noticed that, unlike in the application of Eq. (14) to the baseline structure, Eq. (25) is not valid for calculating the strains of the piezoelectric lead zirconate titanate (PZT) patches when the structure or the patches are modified. The reason is that the patch strains depend on the scalar-point displacement, as implied by Eq. (6), which remains fixed ($\phi_{Hv} = 1$) when the control mode is modified. A practical way to overcome this difficulty is by adding a dummy patch of negligible thickness in parallel to each actual PZT patch, with its grid points connected to the structure side of the patch–structure interface. The modal strains $[\tilde{\phi}_{\epsilon v}]_{\text{dummy}}$ associated with the dummy patches can be calculated by Eq. (25). Since the differences between the modal strains of the actual and dummy patched remain unchanged, the modal strains of the actual patches can then be calculated along the design path by

$$[\tilde{\phi}_{\epsilon v}]_{\text{patch}} = [\tilde{\phi}_{\epsilon v}]_{\text{dummy}} + [\phi_{\epsilon v}]_{\text{patch}} - [\phi_{\epsilon v}]_{\text{dummy}} \tag{26}$$

where $[\phi_{\epsilon v}]_{\text{patch}}$ and $[\phi_{\epsilon v}]_{\text{dummy}}$ relate to the baseline structure.

VI. System Matrix Derivatives

The derivatives of the system matrices in Eqs. (12) and (13) are expressed in [10] as functions of the derivatives of the generalized mass, stiffness, and damping matrices associated with the fixed-basis modes. Similar expressions are presented here for the derivatives of the control-related matrices in $[B_{ae}]$ of Eq. (12). The main difference between the derivatives below and those of [11] is that the control modes here are not fixed, but are functions of the structural design variable. The differentiation of Eq. (15) yields

$$\frac{\partial [\tilde{\phi}_{av}]}{\partial p_k} = [\phi_{av}] \frac{\partial [\psi_{vv}]}{\partial p_k} + [\phi_{ar}] \frac{\partial [\psi_{rv}]}{\partial p_k} + [\phi_{ae}] \frac{\partial [\psi_{ev}]}{\partial p_k} \tag{27}$$

The derivatives in the right side of Eq. (27) are obtained by differentiating Eq. (16), which yields

$$\frac{\partial}{\partial p_k} \begin{bmatrix} \psi_{vv} \\ \psi_{ev} \end{bmatrix} = \begin{bmatrix} \tilde{K}_{vv} & \tilde{K}_{ve} \\ \tilde{K}_{ve}^T & \tilde{K}_{ee} \end{bmatrix}^{-1} \times \left(\begin{bmatrix} \phi_{pv}^T \\ \phi_{pe}^T \end{bmatrix} \frac{\partial [\tilde{K}_{pp}^p]}{\partial p_k} [X_{pv}] - \frac{\partial}{\partial p_k} \begin{bmatrix} \tilde{K}_{vv} & \tilde{K}_{ve} \\ \tilde{K}_{ve}^T & \tilde{K}_{ee} \end{bmatrix} \begin{bmatrix} \psi_{vv} \\ \psi_{ev} \end{bmatrix} \right) \tag{28}$$

and by the differentiation of Eq. (21) which yields

$$\frac{\partial[\psi_{rv}]}{\partial p_k} = -[\tilde{M}_{rr}]^{-1}\left(\frac{\partial[M_{rv}]}{\partial p_k}[\psi_{vv}] + \frac{\partial[\tilde{M}_{rr}]}{\partial p_k}[\psi_{rv}] + \frac{\partial[\tilde{M}_{re}]}{\partial p_k}[\psi_{ev}] + \Delta[M_{rv}]\frac{\partial[\psi_{vv}]}{\partial p_k} + [\tilde{M}_{re}]\frac{\partial[\psi_{ev}]}{\partial p_k}\right) \tag{29}$$

The derivatives of the control-related matrices in Eq. (12) can now be calculated with the derivatives of the mass matrices defined with the baseline modes. The derivatives of the control-related aerodynamic terms in $[B_{ae}]$ are

$$\frac{\partial[\tilde{A}_{hv_i}]}{\partial p_k} = [A_{hv_i}]\frac{\partial[\psi_{vv}]}{\partial p_k} + [A_{hh_i}]\frac{\partial[\psi_{hv}]}{\partial p_k} \tag{30}$$

and

$$\frac{\partial[\tilde{E}_v]}{\partial p_k} = [E_v]\frac{\partial[\psi_{vv}]}{\partial p_k} + [E_h]\frac{\partial[\psi_{hv}]}{\partial p_k} \tag{31}$$

The derivatives of PZT patch stresses and strains are those of the dummy patches, as implied by Eq. (26).

VII. Numerical Example

The procedure for aeroservoelastic modeling with piezoelectric actuation is demonstrated using the aeroelastic model of an unmanned aerial vehicle (UAV). The MSC/NASTRAN aircraft structural model of the UAV right-hand side is shown in Fig. 1. The weight of the model is 152 kg. The span of the wing is 4.0 m and the uniform chord length is 0.55 m. The model contains 459 grid points and 580 structural elements. Symmetric boundary conditions are applied along the fuselage beam.

As detailed in [6], the structural model was modified to include a wing-tip trailing-edge control surface with piezoelectric lead zirconate titanate (PZT) layers patched on the upper and lower skins of the forward half of the control surface, as marked in Fig. 1. The patches were modeled as plies of orthotropic material with large chordwise stiffness relative to the patched skins and negligible spanwise stiffness. The control surface is deflected by a voltage command that extracts the upper patch and contracts the lower one in the X directions of the local coordinate systems where the X axes are in the patch planes, pointing to the trailing edge.

The PZT patch properties used for the numerical example are similar to those available with current technology [2,3]. The Young modulus in the X direction is

$$E_1 = 6.0E^{10}\ \text{N/m}^2$$

the patch thickness is

$$t_1 = 0.267\ \text{mm}$$

its chordwise length is

$$l_c = 52.6\ \text{mm}$$

the free chordwise strain per unit voltage input is

$$\epsilon_x = 1.74\ \mu\text{strain/V}$$

and the maximal voltage input is 1000 V.

To obtain high-accuracy response to piezoelectric control commands, the baseline modes are first calculated with fictitious masses at the patch–structure interface as discussed in [6]. The control mode of static deformations due to unit voltage command was generated in [6] in two ways, by a static solution with the finite-element model, and through normal-modes analysis with the dummy huge mass M_H. Both solutions were based on $\{X_{av}\}$ of Eq. (2) being a zero vector except for the terms $\{x_v\}$ associated with the in-plane X-direction coordinates of the upper patch trailing-edge points, which are

$$\epsilon_x * l_c = 9.15E^{-8}\ \text{m}$$

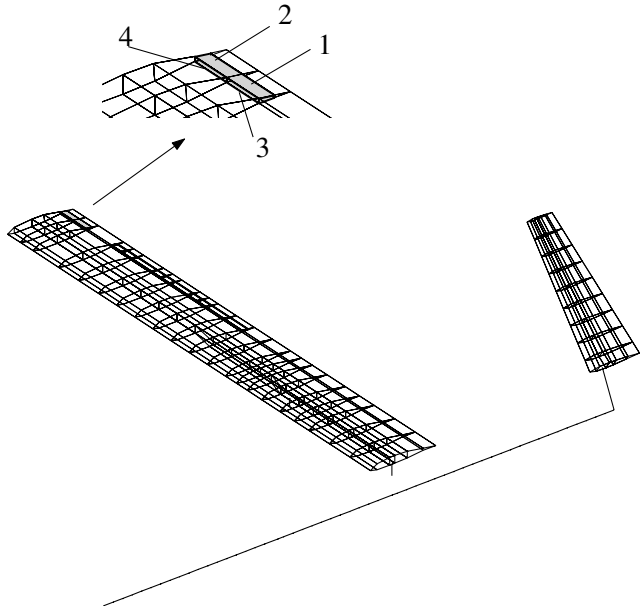

Fig. 1 UAV structural model.

each, and those of the lower patch which are $-9.15E^{-8}$ m each. The two computation methods resulted with identical control modes. The normal-modes method is used below because it is significantly more convenient, as explained above.

The modal solution is performed by duplicating the patch–structure interface points, adding a scalar point and imposing the MPC constraints of Eq. (5) and loading the scalar point by the dummy mass $M_H = 10^6$ kg. The resulting frequencies and modes are practically identical to those of the baseline structure, except that the modes include now the control mode with practically zero frequency. Since the calculated control mode is normalized to unit generalized mass, it should be multiplied by 10^3 in order to obtain the actual control mode. With maximal electric input of 1000 V, the control-surface deflection is 0.67°.

The aerodynamic boxes of the doublet-lattice unsteady aerodynamic model are shown in Fig. 2 with the locations of 4 accelerometers for subsequent ASE analysis. More details are given in [6]. The generalized aerodynamic matrices served as tabulated data for the rational aerodynamic approximation of Eq. (11). The approximation was performed by the ZAERO code [5] with 6 aerodynamic lag terms, physical weighting of the tabulated data, and with the steady aerodynamics constrained to match the data at $k = 0$. The approximation coefficients were then used by ZAERO to construct the state-space model of Eqs. (12) and (13). The model has 52 structural states and 6 aerodynamic states. The output equations were set up to provide the displacement and acceleration at Accelerometer 1, the chordwise strains in the four PZT elements and those in one of the composite layers of the skin elements to which the PZT elements are patched. The state-space matrices were exported to Matlab for the remaining analyses in this work.

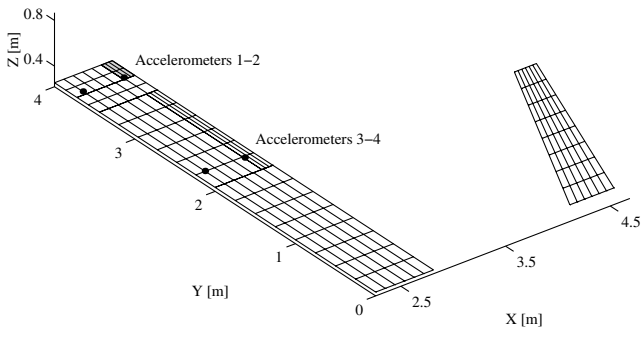

Fig. 2 UAV aerodynamic model.

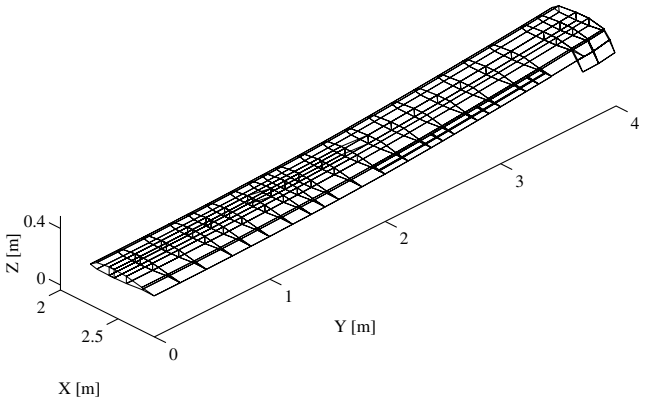

Fig. 3 Static response with aerodynamic forces.

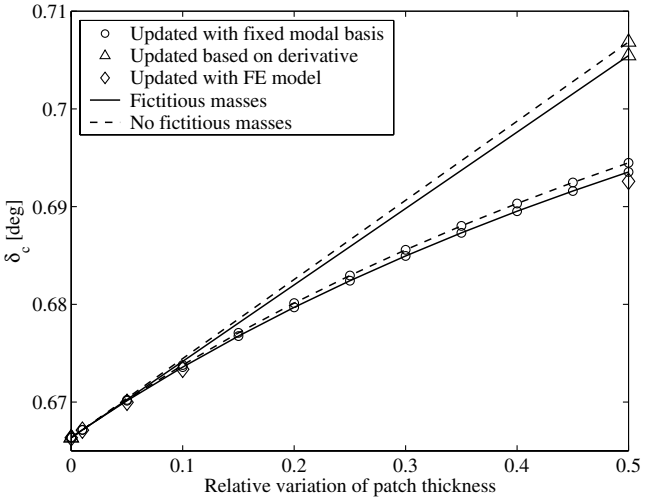

Fig. 4 Control-surface angle vs added PZT patch thickness.

Static and dynamic response characteristics with the direct-force and the control-mode approach were demonstrated in [6]. The approach taken in this paper is the control-mode approach, which was found to be more robust and convenient. The fictitious masses that generate the local modes were not essential in the control-mode applications of [6]. Their effectiveness in sensitivity analysis is examined below.

The sensitivity model is first demonstrated by calculating the steady-state response to a static piezoelectric command of 1000 V at airspeed $V = 50$ m/ sec. The deformed wing shape with the deformations multiplied by 100, is shown in Fig. 3. Variations of the control-surface deflection angle with added thickness to the PZT patches between 0 and 0.5 of the original thickness are shown in Fig. 4. It can be observed that the estimated changes in the control-surface deflection based on the fixed-mode approach, without returning to the finite-element model, are very close to those obtained by generating new models from updated finite-element models. The derivatives calculated for the baseline model are accurate, but their use in predicting the response with added PZT thickness is quite limited. It can be also observed that the model is considerably less accurate when fictitious masses are not used, but may still be sufficiently accurate under certain move limits. Similar results are shown in Fig. 5 for the aeroelastic displacements at the wing-tip area (accelerometer no. 1).

The variations of the chordwise strains in PZT patch no. 1 with the relative increase of the patch thickness are shown in Fig. 6. Here the effect of the fictitious masses is larger. Whereas the strains predicted with fixed-modal-basis approach and fictitious masses are almost identical to those obtained with a full model update, the incremental changes are about 10% off when fictitious masses are not used.

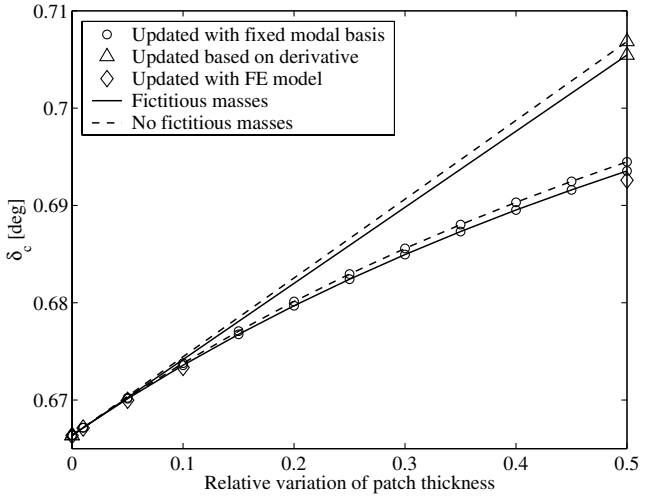

Fig. 5 Static wing-tip displacement vs added PZT patch thickness.

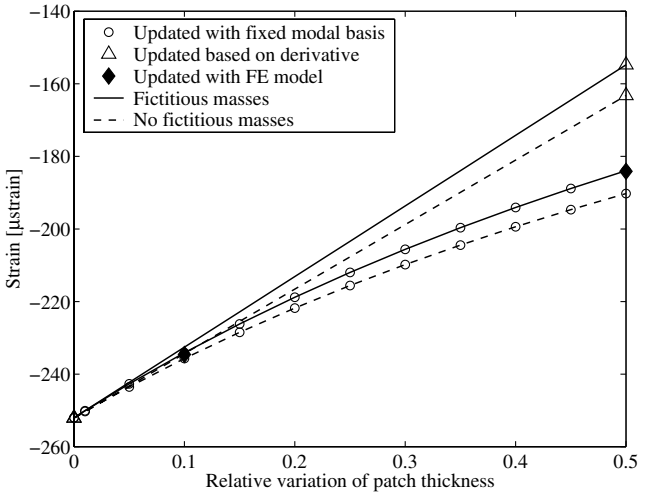

Fig. 6 Strains in a PZT patch vs added PZT patch thickness.

VIII. Conclusions

A modal-based method for obtaining state-space equations of motion for aeroservoelastic analysis with strain actuators was expanded in this work to include the calculation of stability and response sensitivities associated with the actuator parameters. The state-space equations were developed with the control-mode approach. The procedure for obtaining the control modes was defined such that they can be conveniently generated together with the regular vibration modes using standard normal-modes procedures. The strains in the piezoelectric elements appear in these modes with the piezoelectric control effects included. The analysis model was expanded to facilitated efficient aeroservoelastic optimization with a fixed modal basis, taking into account changes in the control mode due to the updated elastic equilibrium. The technique of adding fictitious masses to improve the local accuracy around the piezoelectric patches improves the accuracy of PZT-related sensitivity analysis and may be used to expand the move limits in optimization studies with reduced-order models. The models are formulated such that it can be constructed using common finite-element and aeroservoelasticity codes such as MSC/NASTRAN and ZAERO.

Acknowledgment

The work presented in this paper is partly financed by the European Union through the project Active Aeroelastic Aircraft Structures (3AS), Project Number G4RD-CT-2002-00679.

References

[1] Crawley, E., "Intelligent Structures for Aerospace: A Technology Overview and Assessment," *AIAA Journal*, Vol. 32, No. 8, August 1994, pp. 1689–1899.

[2] Chopra, I., "Review of State of Art of Smart Structures and Integrated Systems," *AIAA Journal*, Vol. 40, No. 11, November 2002, pp. 2145–2187.

[3] Forster, E., and Livne, E., "Integrated Design Optimization of Strain Actuated Structures for Dynamic Shape Control," AIAA Paper 2000-1366, 2000.

[4] Karpel, M., "Time Domain Aeroservoelastic Modeling Using Weighted Unsteady Aerodynamic Forces," *Journal of Guidance, Control, and Dynamics*, Vol. 13, No. 1, 1990, pp. 30–37.

[5] ZAERO Version 7.0 Theoretical Manual, ZONA 01-24.4, ZONA Technology, Scottsdale, AZ, June 2001.

[6] Karpel, M., and Moulin, B., "Models for Aeroservoelastic Analysis with Smart Structures," *Journal of Aircraft*, Vol. 41, No. 2, 2004, pp. 314–321.

[7] Karpel, M., and Newman, M., "Accelerated Convergence for Vibration Modes Using the Substructure Coupling Method and Fictitious Coupling Masses," *Israel Journal of Technology*, Vol. 13, No. 1, 1975, pp. 55–62.

[8] Karpel, M., and Raveh, D., "Fictitious Mass Element in Structural Dynamics," *AIAA Journal*, Vol. 34, No. 3, 1996, pp. 607–613.

[9] Karpel, M., Moulin, B., and Chen, P. C., "Extension of the g-Method Flutter Solution to Aeroservoelastic Stability Analysis," *Proceedings of the 44rd AIAA/ASME/ASCE/AHS/ASC Structures, Structural Dynamics and Materials Conference, Norfolk, Virginia, U.S.A., April 2003*, AIAA Paper 2003-1512; *Journal of Aircraft* Vol. 42, No. 3, 2005, pp. 789–792.

[10] Karpel, M., "Multidisciplinary Optimization of Aeroservoelastic Systems Using Reduced-Size Models," *Journal of Aircraft*, Vol. 29, No. 5, 1992, pp. 939–946.

[11] Idan, M., Karpel, M., and Moulin, B., "Aeroservoelastic Interaction Between Aircraft Structural and Control Design Schemes," *Journal of Guidance, Control, and Dynamics*, Vol. 22, No. 4, 1999, pp. 513–519.